Electronic Supplementary Material (ESI) for Nanoscale.


Supporting Information

# $MoTe_2$ van der Waals Homojunction p-n Diode with Low Resistive Metal Contacts

Sikandar Aftab, Muhammad Farooq Khan, Praveen Gautam, Hwayong Noh, and Jonghwa Eom*

Department of Physics & Astronomy and Graphene Research Institute–Texas Photonics Center International Research Center (GRI–TPC IRC), Sejong University, Seoul 05006, Korea

*Corresponding author: eom@sejong.ac.kr

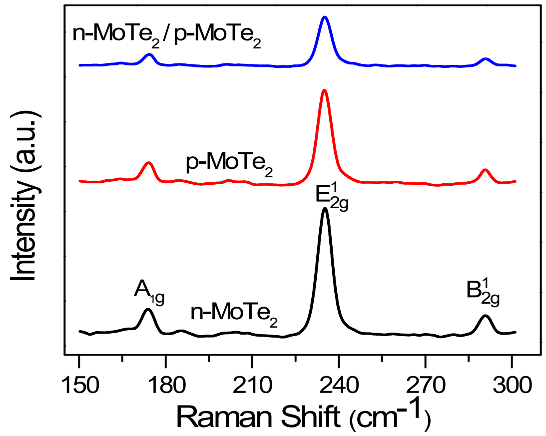


**Figure S1.** Raman spectra of n-$MoTe_2$, p-$MoTe_2$, and p-$MoTe_2$/n-$MoTe_2$ heterostructures.

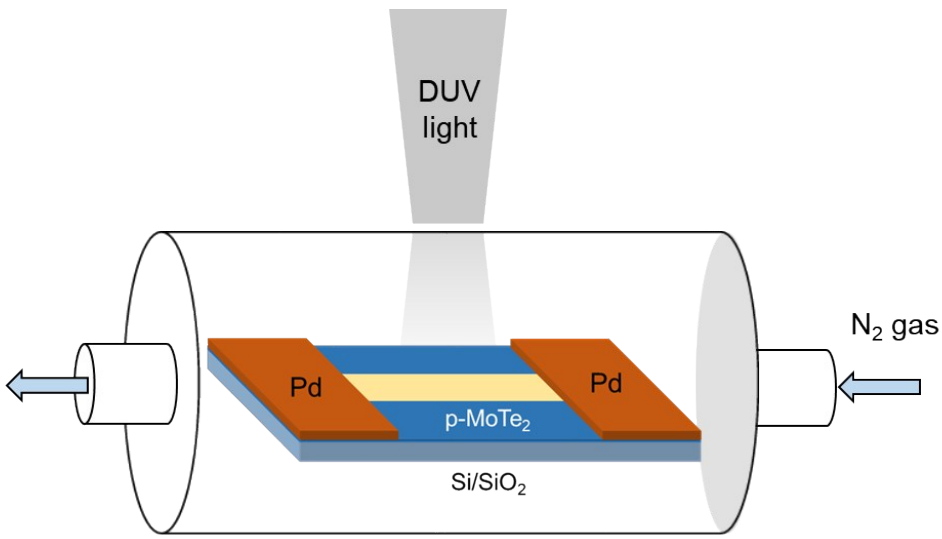


**Figure S2.** Schematic illustration of p-$MoTe_2$ FET when employing same metal contacts under DUV light of average intensity 11 $mW/cm^2$ and wavelength 220 nm, inverted to n-$MoTe_2$ FET.

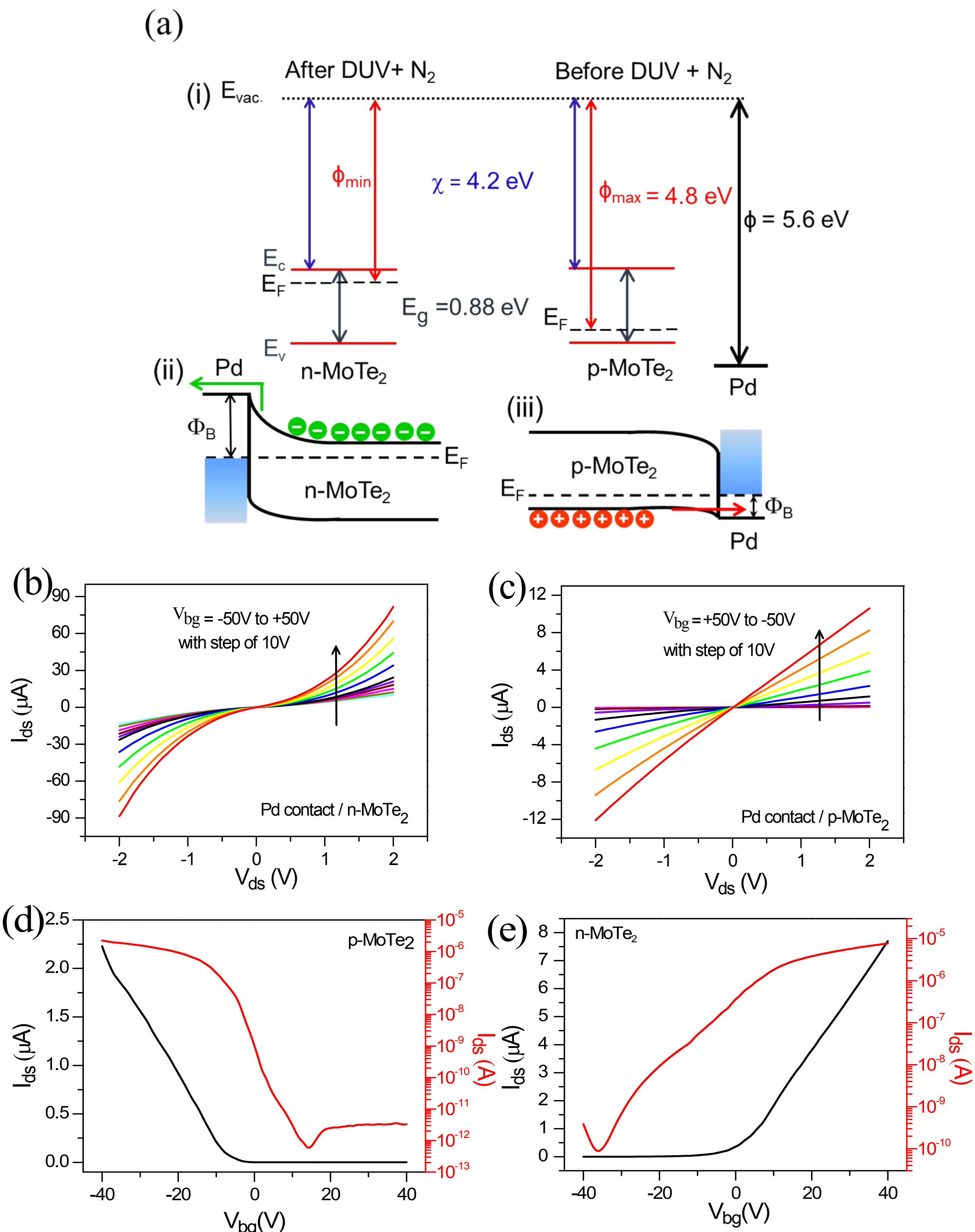
(a)
(i) E_vac.
After DUV+ N2
Before DUV + N2
ϕmin
χ = 4.2 eV
ϕmax = 4.8 eV
ϕ = 5.6 eV
Ec
EF
Eg =0.88 eV
EF
Ev
n-MoTe2
p-MoTe2
Pd
(ii)
Pd
ΦB
EF
n-MoTe2
(iii)
p-MoTe2
EF
ΦB
Pd
(b)
Vbg = -50V to +50V
with step of 10V
Pd contact / n-MoTe2
Ids (μA)
Vds (V)
(c)
Vbg = +50V to -50V
with step of 10V
Pd contact / p-MoTe2
Ids (μA)
Vds (V)
(d)
p-MoTe2
Ids (μA)
Ids (A)
Vbg(V)
(e)
n-MoTe2
Ids (μA)
Ids (A)
Vbg(V)

**Figure S3.** (a) (i) Band structure of p-$MoTe_2$ and n-$MoTe_2$ before and after DUV+$N_2$ treatment, respectively. Band diagram: (ii) Schottky and (iii) Ohmic contact effect of n-$MoTe_2$ and p-$MoTe_2$ with Pd, respectively. $I_D$-$V_D$ characteristics of (b) n-$MoTe_2$ and (c) p-$MoTe_2$ as a function of $V_{bg.}$ (d) Transfer characteristics of p-$MoTe_2$ before DUV+$N_2$ treatment of the same device with $V_{ds}$= 0.5 V. The right axis shows transfer characteristc in log scale. (e) Transfer characteristics of n-$MoTe_2$ after DUV+$N_2$ treatment of the same device with $V_{ds}$= 0.5 V. The right axis shows transfer characteristc in log scale.

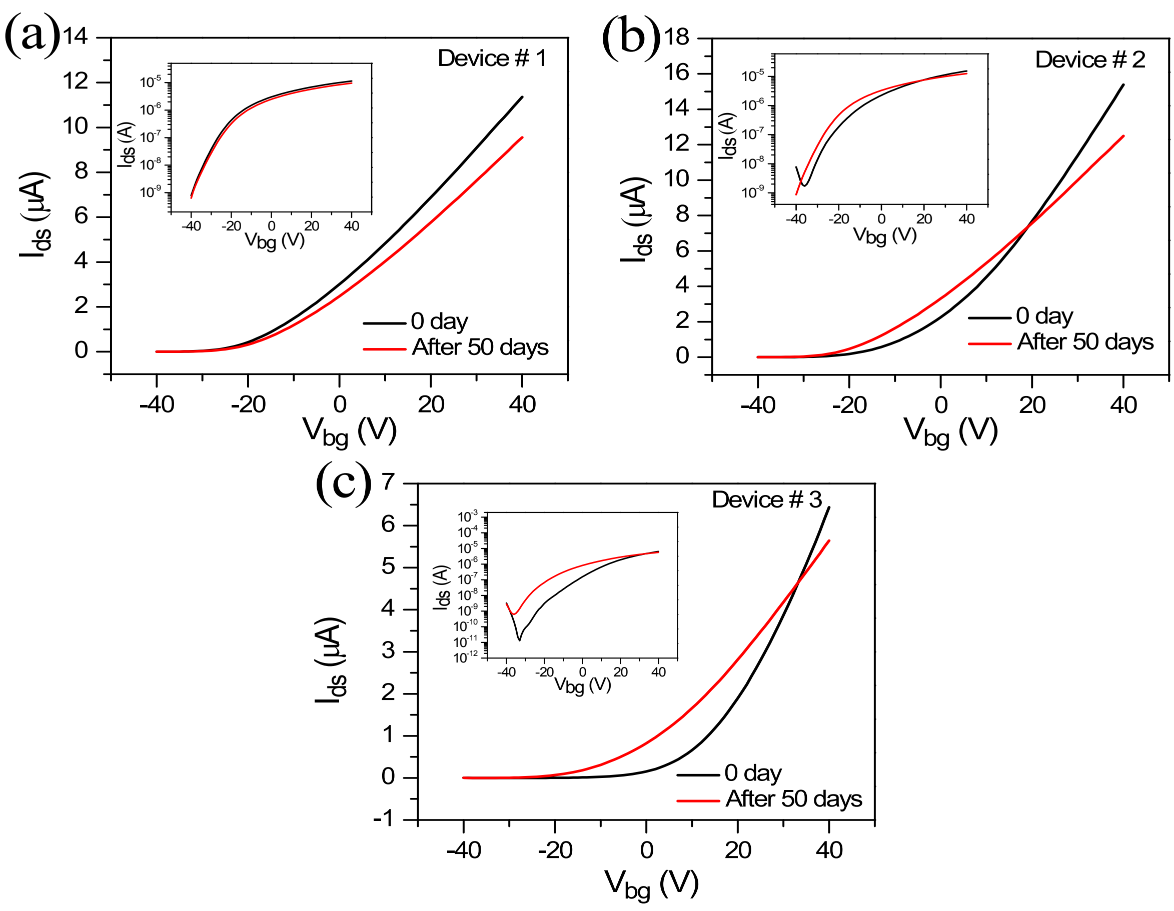


**Figure S4.** Transfer characteristics of n-$MoTe_2$ after DUV+$N_2$ treatment of (a) device #1 (b) device #2, and (c) device #3 at $V_{ds}$= 0.5 V, showing the stability of the devices in an atmospheric environment. Inset shows transfer characteristcs in log scale.

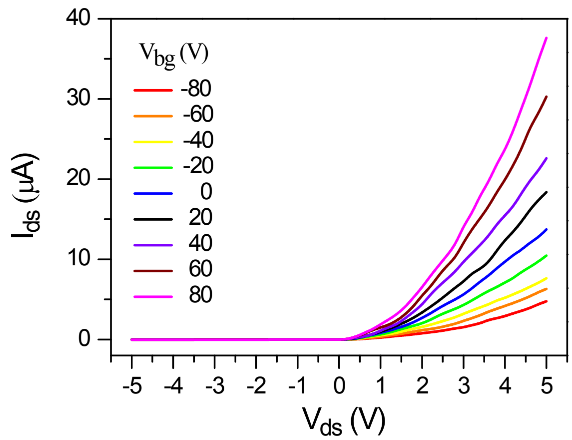


**Figure S5.** Gate-dependent rectifying effect of the $MoTe_2$ homojunction p-n diode in linear scale.

**Electrical rectifying property of $MoTe_2$ by employing unlike metal contacts:**

In this study, we found that the output characteristics with a combination of different metal contacts (as shown in Figure S6(a)) showed a clear rectifying behavior due to the Schottky junction formed upon contact[1] with an on/off ratio of up to $10^2$, and a particularly strong rectification effect for negative gate biases, as shown in Figure S6. This is due to the Schottky barrier height between Al and p-$MoTe_2$, as Al metal has a low work function value (~4.1 eV)[2], which does not exceed the valence band maximum or the Fermi level (~4.7-4.99 eV) for p-type $MoTe_2$ based on theoretical calculations[3]. Thus, Al forms a Schottky junction with p-$MoTe_2$, whereas the Pd electrode forms ohmic contacts with p-$MoTe_2$ owing to its higher work function value (~5.6 eV)[4]. The value of $\Phi_B$ according to the Schottky–Mott rule is related to the change in work function value of the metal and the electron affinity of the semiconductor, i.e., $\Phi_B = \Phi_{metal} - \chi_{semi}$. Nevertheless, some semiconductors do not comply with this rule for the formation of metal-induced gap states[5, 6], which fill with electrons, thereby pinning the center of the band gap closer to the Fermi level. This influence is termed as Fermi-level pinning[4, 7],

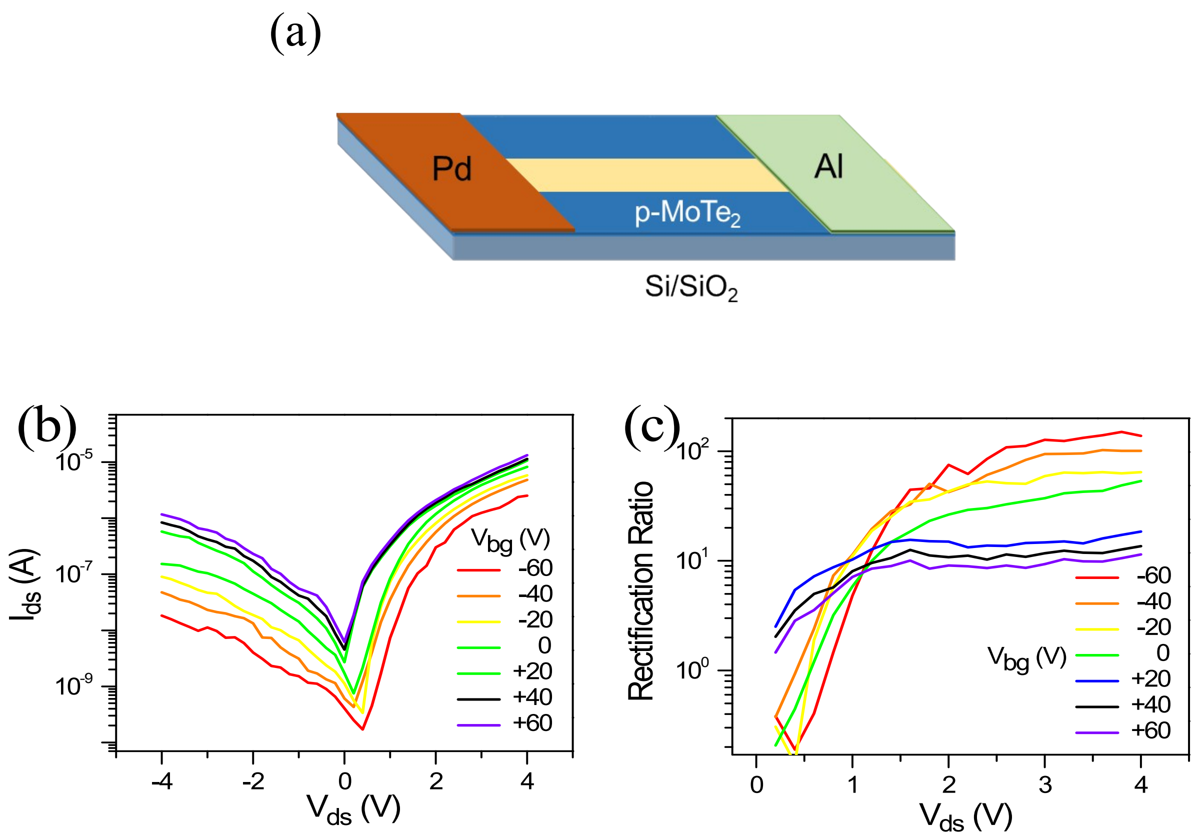


**Figure S6.** (a) Schematic illustration of p-$MoTe_2$ FET when employing a combination of different metal contacts (Pd and Al). Gate-dependent (b) rectifying effect (c) rectification ratio of the $MoTe_2$ flake with Pd and Al source and drain electrodes in the log scale.

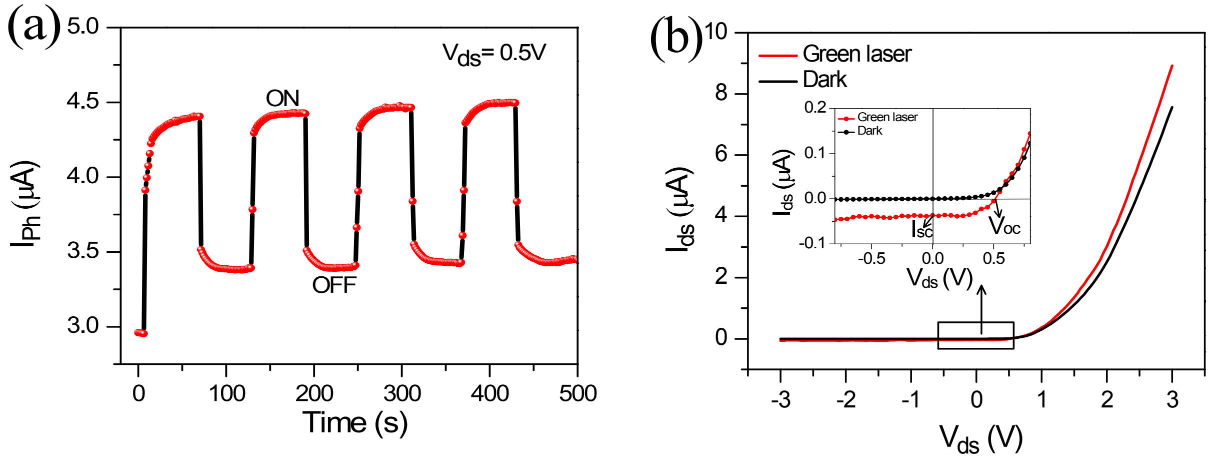


**Figure S7.** Photoresponse of $MoTe_2$ homojunction p-n diode. (a) Photocurrent of the $MoTe_2$ homojunction p-n diode with green laser light illumination between the ON and OFF states. (b) $I_D$-$V_D$ characteristics of the device with and without light illumination at zero gate bias (λ = 530 nm, $P_{Laser}$= 50 mW/cm$^2$). The inset in (b) shows the open circuit voltage ($V_{oc}$) and short circuit current ($I_{sc}$) under green laser light.

**Two breakdown phenomena in the $MoTe_2$ homojunction p-n diode:**

When a diode operates in the reverse biased region, a very small leakage current flows, and thus, it acts as an open circuit[8]. The reverse leakage current increases suddenly due to the rise in reverse bias voltage, and consequently, dynamic resistance becomes too low. This bias voltage is identified as reverse breakdown voltage[8]. During Zener breakdown, the p and n materials become heavily doped creating a smaller barrier height between them, due to which quantum tunneling can occur. Therefore, electric field existing across the potential barrier is sufficient to overcome the barrier height, causing band-to-band tunneling and current flow at a low reverse bias voltage[8, 9]. Avalanche breakdown causes high electrostatic field interrelated with p and n regions under low p-n diode doping, and the barrier height is intermediate. Both breakdown phenomena may occur under a reverse bias voltage, as shown in Figure S8. We note that the temperature coefficient of Zener breakdown is negative, whereas the temperature coefficient of avalanche breakdown voltage is positive.

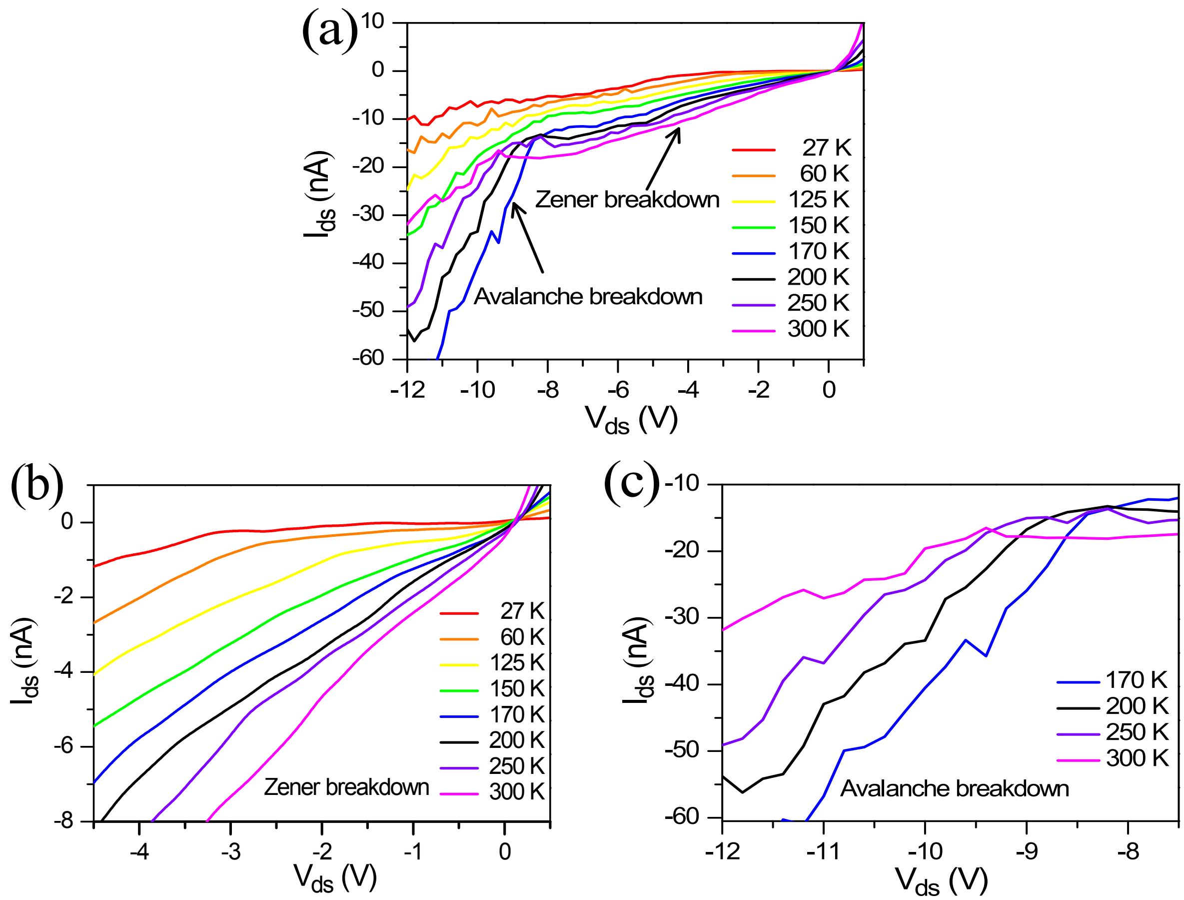


**Figure S8.** (a) *I-V* characteristics at different temperatures at $V_{bg}$ = 0 V. (b) Extended *I-V* characteristics showing Zener breakdown. As the temperature increases, the magnitude of Zener breakdown voltage decreases. (c) Extended *I-V* characteristics showing avalanche breakdown. As the temperature increases, the magnitude of avalanche breakdown voltage increases.

**References**

1. N. J. Townsend, I. Amit, M. F. Craciun and S. Russo, *2D Materials*, 2018, **5**, 025023.

2. M. W. Iqbal, M. Z. Iqbal, M. F. Khan, M. A. Shehzad, Y. Seo, J. H. Park, C. Hwang and J. Eom, *Scientific reports*, 2015, **5**, 10699.

3. J. Kang, S. Tongay, J. Zhou, J. Li and J. Wu, *Applied Physics Letters*, 2013, **102**, 012111.

4. C. Kim, I. Moon, D. Lee, M. S. Choi, F. Ahmed, S. Nam, Y. Cho, H.-J. Shin, S. Park and W. J. Yoo, *ACS nano*, 2017, **11**, 1588-1596.

5. K.-A. Min, J. Park, R. M. Wallace, K. Cho and S. Hong, *2D Materials*, 2016, **4**, 015019.

6. S. Picozzi, A. Continenza, G. Satta, S. Massidda and A. Freeman, *Physical Review B*, 2000, **61**, 16736.

7. P. Bampoulis, R. Van Bremen, Q. Yao, B. Poelsema, H. J. Zandvliet and K. Sotthewes, *ACS applied materials & interfaces*, 2017.

8. B. Van Zeghbroeck, *Colarado University*, 2004.

9. P. Horowitz, W. Hill and I. Robinson, *The art of electronics*, Cambridge university press Cambridge, 1980.